ARQII Publication
http://arqiipubl.com/ams
APPLICATIONS OF
MODELLING AND SIMULATION
eISSN 2600-8084
VOL 5, 2021, 102-114

Port Flow Simulation and In-cylinder Swirl Motion Characteristic Effects in Internal Combustion Engine Duty Cycle

Aniekan Essienubong Ikpe*, Ikechukwu Bismarck Owunna and Philip Obhenime John

Department of Mechanical Engineering, University of Benin, P.M.B. 1154, Nigeria

*Corresponding author: aniekan.ikpe@eng.uniben.edu

Submitted 27 January 2021, Revised 21 February 2021, Accepted 02 March 2021.

Abstract: Combustion process in internal combustion engines involve significant temperature and pressure, carbon deposit, turbulence flame, swirling and tumbling flows which are considered necessary for operating these engines. This study examines the in-cylinder effects of swirling and tumbling motion along with the in-cylinder temperature during combustion process of air-fuel mixture. A detailed port flow analysis was carried out using ANSYS R-16 software and a valve lift of 8 mm. The velocity magnitude and mass flow rate were monitored using swirl motion simulated profiles and cut planes. Motion analysis was carried out to determine the angular velocity of the cycle using SOLIDWORKS 2017. The average angular velocity of the crankshaft was found to be 1315 rpm, with percentage deviation of less than 20%. It was also found that the area-weighted average velocity of charge was 11 m/s with corresponding mass flow rate measured as -0.055479 kg/s. The maximum flow rate was calculated at 8 mm as 0.005417 kg/s. The ICE swirl plane 1, 2 and 3 were characterized by different contours of velocity magnitude, indicating that the swirl intensity increased as the charge moved further down the cylinder while the charge volume of swirl increased along the cylinder length. For the ICE cut plane, the velocity increased as the swirl increased while the mass flow rate decreased as the fluid went further away from the poppet valve. Therefore, the intensity of swirl increased along the stroke length of the engine cylinder. In addition, increase in the swirl number led to uniform radial temperature distribution as well as reduction in the in-cylinder flame temperature which can mitigate against the formation of toxic pollutants.

Keywords: Air-fuel; In-cylinder combustion; Internal combustion engine; Port flow simulation; Swirl motion.

1. INTRODUCTION

Since 1876 when Nicolaus A. Otto developed the spark-ignition engine, through 1892 when Rudolf Diesel invented the compression-ignition engine [1], till recent times, automobile industries have been driven by the cravings for effective performance, better fuel efficiency and less emissions. However, the working principles of Internal Combustion Engine (ICE) over the years have not changed significantly despite all the reforms and developments. It operates by sucking in some air while the engine is engaged, compressing it to the smallest volume, mixing it with fuel and burning it inside the cylinder (combustion chamber) and ejecting hot gases from the hot air-fuel combustion with extremely high force [2, 3]. The in-cylinder air-fuel mixture upon burning changes into hot gases which impacts on the piston and causing reciprocating motion which in the process is converted into rotary motion of the crank shaft [4]. At this stage, the reciprocating piston transfer the forces resulting from the expanding gas to the crankshaft through the connecting rod [5, 6].

The in-cylinder flow dynamics of ICE is classified into three major categories namely: swirl, tumble and squish. The in-cylinder flow rotational axis is parallel to the cylinder axis during swirl motion while tumble is characterised by the flow with an axis perpendicular to the axis of the piston motion in the cylinder. On the other hand, squish is a radial flow occurring at the end of the compression stroke towards the center-line of the cylinder [7]. Studies have shown that large scale flow configurations such as swirl and tumble has a high tendency of increasing turbulence level at the time of ignition, as a result, significantly affecting both pollutant emissions and fuel efficiency [8, 9]. However, swirl at the end of compression and beginning of combustion breaks into turbulence motion due to upward motion of the piston. In addition, studies have also revealed that high levels of swirl does not improve combustion and emission; rather, it reduces the volumetric efficiency as swirl created reduces the kinetic energy of the flowing fluid [10, 11].

During the intake stroke, flow generation with intense vorticity (swirl and/or tumble) in the cylinder is an effective tool for achieving a great intensity of turbulence which can be maintained during the compression stroke. The stability of these swirling motion enables the engine to maintain a significant level of turbulence during the fuel injection phase and induce

optimal conditions for the initiation and the development of the combustion process [12, 13]. During the compression stroke, swirl vortex can enhance turbulence flow through the following methods: Turbulence generated by shear at the wall is transported throughout the bulk of flow by diffusion. Also, swirl generated secondary flow develops turbulence through shear and vortex shedding or swirl vortex in combination with the squish flow which causes an acceleration of the rotational speed of the vortex as the piston approach Top Dead Centre (TDC) to conserve the angular momentum [14, 15].

Quantitative representations of the in-cylinder flow field during compression consist of swirl and tumble numbers, and in some studies, fluctuation from the cycle mean [16, 17]. However, a dimensionless parameter known as the swirl ratio is used in quantifying swirl motion within the cylinder [18]. In other words, swirl is the rotation of charge also referred to as air-fuel supply within the cylinder axis, and its application in SI engines is to enhance combustion rate and in diesel engines to control the rate of air-fuel mixture. Ramanjulu et al. [19] reported that the in-cylinder swirl dynamics increases the IC engine performance and as well decreases the emission level. Parameters like engine speed, manifold, combustion chamber configuration etc. has direct influence on the in-cylinder swirl characteristics, as it plays a vital role in mixing air and fuel inside the cylinder for effective combustion [20]. Therefore, intake manifold and cylinder head of ICEs must be designed accurately in order to minimize the flow resistance and optimise the swirl effects [21, 22].

Santavicca effects of swirl and tumble on mixture preparation during cold start of a gasoline direct-injection engine was investigated by Lee et al. [23]. The results revealed that both swirl and tumbling motions enhanced the rate of fuel vaporization and air-fuel mixing, which resulted in better cold start performance. Furthermore, swirl and tumbling motions were also reported to adequately retard ignition timing as it has faster burning, which offers ample time for fuel vaporization and air-fuel mixing prior to being ignited. El-Adawy et al. [24] experimentally studied an ICE cylinder flow under steady-state conditions. In the first experiment, the impulse torque meter method (Ricardo) was used while paddle wheel measuring technique in Forschungsgesellschaft für Energietechnik und Verbrennungsmotoren (FEV) was employed in the second experiment. At higher valve lifts a strong tumble motion was generated with high values of non-dimensional rig-tumble, average turbulent kinetic energy and vorticity magnitude. Full velocity vector maps were obtained in one vertical (tumble) plane (passing through the centre of the cylinder, which was located between the two intake valves) at different valve lifts including 2 mm, 5 mm, 8 mm and 9 mm.

Kumar and Nagarajan [25] experimentally investigated the in-cylinder swirling flow of a spark ignited engine. Variations in diverse non-dimensional parameters such as swirl ratio and flow coefficient at different throttle opening and valve lifts were studied using a steady-state flow bench. From the results obtained, higher swirl ratios and swirl coefficients can be achieved with shrouded valves and twisted tapes but at the expense of the flow coefficient. To study the effect of valve lift on the flow of fluid inside the cylinder, Kumar and Jayashankar [26] developed an ICE with inlet port diameter 46 mm, valve diameter 43 mm and the length and diameter of the cylinder is 562 mm and 93.65 mm. The CFD simulation indicated that valve lift affects velocity flow field inside the cylinder. As the valve lift increased, flow separation becomes critical because, as valve lift increases losses near the valve also increase.

Akele et al. [27] performed port flow analysis on ICE to determine flow rate and swirl at different valve lift under stationary engine parts. The model geometry was developed using ANSYS Design modeller for one cylinder, one suction port and one exhaust port, and two valves while CFD software that uses the finite volume method of numerical analysis to solve continuity equation was used for the port flow simulation. It was observed that air mass characterised by swirling motion was more concentrated around the valve and inlet port cross-section. It was also observed that air stream experienced turbulence as it flowed downwards inside the cylinder, swirling air stream was turbulent as it flowed towards the cylinder walls where it experienced tumbling which enhances smooth combustion and the mass flow rate of inlet air increased with valve lift. Whitelaw and Xu [28] compared the cyclic variations in combustion process in terms of the maximum pressure, flame speed and in cylinder flow velocity without and with an intake valve shroud. This led to increase in both the tumble and swirl ratios in the spark ignition engine investigated. The photographic analysis confirmed the dominant effect of swirling flow on flame propagation and deviations of the flame kernel from spherical plane as the air-fuel ratio increased with much higher probability of influence of velocity fluctuations.

This study is focused on the port flow simulation and in-cylinder swirl motion characteristic effects in ICE duty cycle. It serves as a guide to understanding of air-fuel mixture flow dynamics for optimum engine combustion, performance and efficiency based on the principles of swirl and tumble flows which influences air streams entering the cylinder at intake stroke while enhancing the mixing rate of air and fuel during compression stroke.

2. MATERIALS AND METHODS

The conventional four stroke engine has an additional air intake and air compression stroke. The engine and the test environment was modelled in SOLIDWORKS 2017. The engine was a Nissan Primera inline engine assumed to be operating on a four stroke cycle. The motion tests were carried out from the power generated from the combustion stroke and the energy spent on all other strokes. A flywheel was used to store the excess energy generated during the power stroke. This study examines the vertical displacement of the piston, power, momentum and trace paths over a period of six seconds. The results are plotted with the parameter plotted against time. The model was reduced from a full design to the test design. The full design shows the details of the design but the test prototype contains only the components required for analysis arranged in such a way that their motion properties can be tested. The ICE model and test prototype is presented in Figure 1 while Figures 2-5 show full ICE model components (piston head, connecting rod, flywheel and crankshaft).

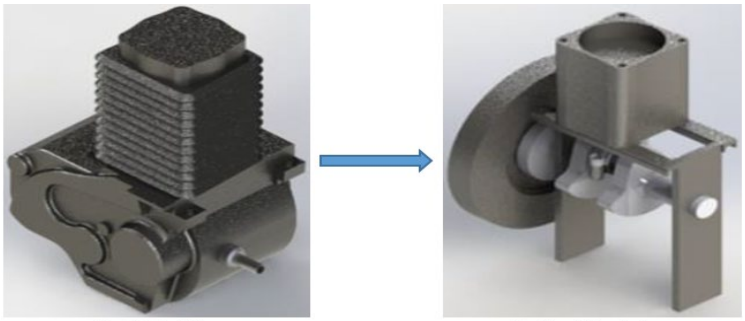

a. Full Model b. Test Prototype

Figure 1. Full ICE model and test prototype

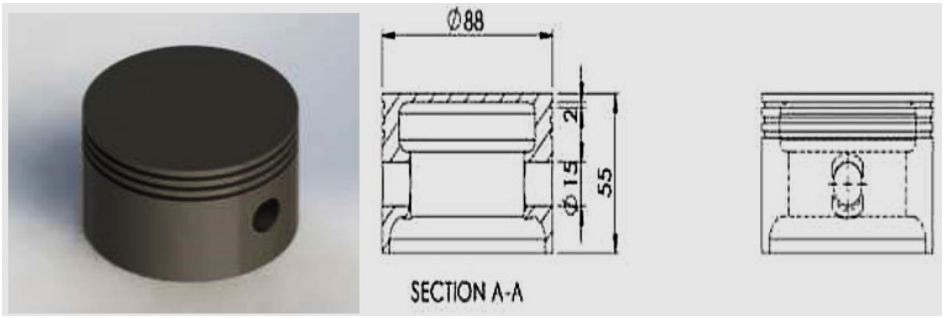

Figure 2. ICE piston head assembly

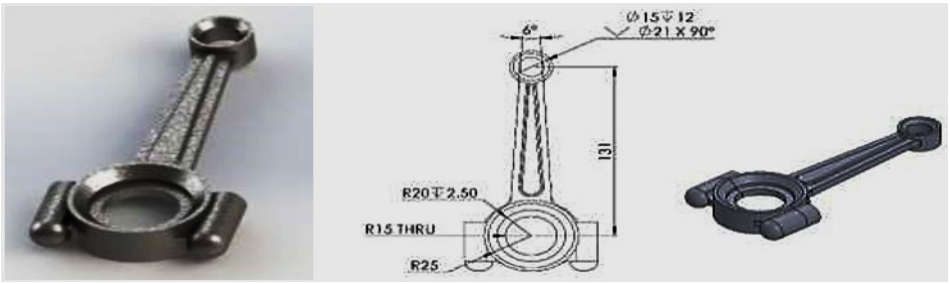

Figure 3. ICE connecting rod assembly

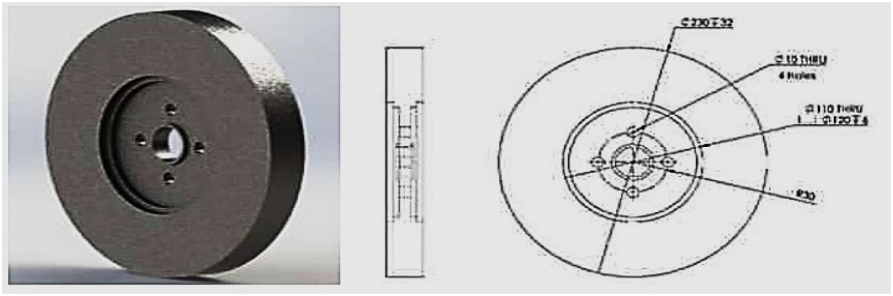

Figure 4. ICE flywheel rod assembly details

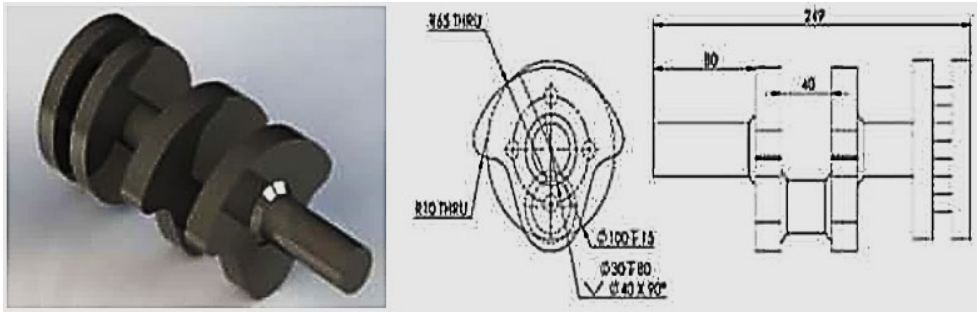

Figure 5. ICE crankshaft assembly details

2.1 Internal Force

A force function was applied to the face of the piston which signified the power generated or expended during each stroke. Calculations were carried out to convert the power at each stroke to mechanical forces which were applied as segmented forces on the piston face at specific timing. The calculation was done for power stroke, compression stroke and the second power stroke.

Power stroke:
Given the pressure of combustion as 72 bar (7200000 N/m^2), bore of cylinder as 88 mm, and radius as 44 mm, the force (Pressure × Area) can be obtained as 4379 N.

Compression stroke:
With the pressure of combustion as 6.65 bar (665625 N/m^2), the force can be obtained as 4047 N.

Second power stroke:
With the pressure as 22 bar (2217033 N/m^2), the force can be obtained as 13484 N.

The forces during the intake and exhaust stroke were ignored due to their insignificant value and therefore assumed to be zero.

2.2 ANSYS Port Flow Simulation Report

The model domain was ice-fluid port, and total node number of 4888073 with 9041200 elements. Boundary physics for ICE, boundary conditions adopted for the model simulation, relaxation and pressure-velocity coupling and the discretization scheme are presented in Table 1 respectively. The method of solution employed in analyzing and solving the ICE port flow simulation was CFD in ANSYS R-16 software, which used the finite volume method of numerical analysis to solve the continuity, Navier-Stokes and energy equations governing the air medium in the ICE cylinder [29]. The software performed geometry check, geometry preparation, mesh generation as well as solver setup up and automatically created the default swirl plane from geometry information, and defined custom field functions for the swirl planes. Figure 6 shows the ICE model and visualization information and Figure 7 represents schematics showing flow movement. The operating parameters employed in the ICE port flow simulation are presented in Table 1. The momentum conservation equation for swirl velocity is given by Equation (1). The strength of the swirl is determined by the swirl number (S_n) given by Equation (2) while the ratio of axial flux of tangential momentum to the axial flux of axial momentum times the effective nozzle radius is known as swirl intensity (S_i) expressed in Equation (3). The equations for pseudo transient, following the mass, momentum and energy equations are given by Equations (4) – (6).

Table 1. Parameters for the ICE model

Engine parameters and parameters used for the simulation			
Engine parameters	Values	Simulation parameters	Values
Compression Ratio	9.3:1	Opening area	0.5 mm
Stroke	68 mm	Air pressure	1.65 bar
Bore	88 mm	Air temperature	360 K
Displacement	2500 cc	Engine speed	3000 rpm
Con rod length	122.5	Air to fuel ratio	14.6:1
Swept volume	499.5 cm^3	Inlet valve open	330º BTDC
Crank shaft bearing	7	Inlet valve close	610º BTDC
Number of valves	4	Squish height at TDC	1.1 mm
Maximum power output	148 bhp or 110 kw	% Squish area	10.8

Boundary Conditions		
Type	Zones	Values
pressure-outlet	ice-outlet	Gauge Pressure, 5000 Pa
		Backflow Total Temperature, 300 K
pressure-inlet	ice-inlet-inplenum1	Gauge Total Pressure, 0 Pa
		Supersonic/Initial Gauge Pressure, 0 Pa
		Total Temperature, 300 K
wall	wall-ice-fluid-port	Temperature, 300 K
wall	ice-cyl	Temperature, 300 K
wall	ice-slipwall-inplenum1	Temperature, 300 K

wall	ice-slipwall-outplenum	Temperature, 300 K
wall	ice-valve-proximity-faces	Temperature, 300 K

Relaxation and Pressure-Velocity Coupling			
Relaxation		Pressure-Velocity Coupling	
Variable	Relaxation Factor	Type	Coupled
Density	1.000 kg/m^3	Pseudo Transient	Yes
Body Forces	1.000	Explicit momentum under-relaxation	0.500
Turbulent Kinetic Energy	0.750 J/kg	Explicit pressure under-relaxation	0.500
Specific Dissipation Rate	0.750 m^2/s^3		
Turbulent Viscosity	1.000 Ns/m^2		
Energy	0.750 Nm		

Discretization Scheme	
Variable	Scheme
Pressure	Standard
Density	Second Order Upwind
Momentum	Second Order Upwind
Turbulent Kinetic Energy	First Order Upwind
Specific Dissipation Rate	First Order Upwind
Energy	Second Order Upwind

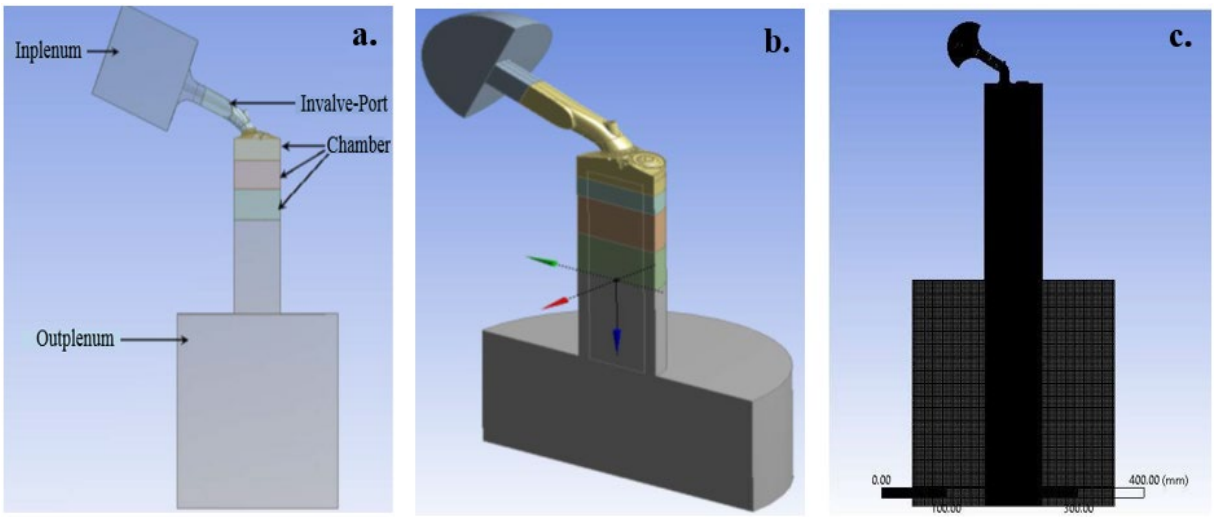

Figure 6. ICE model and mesh visualization

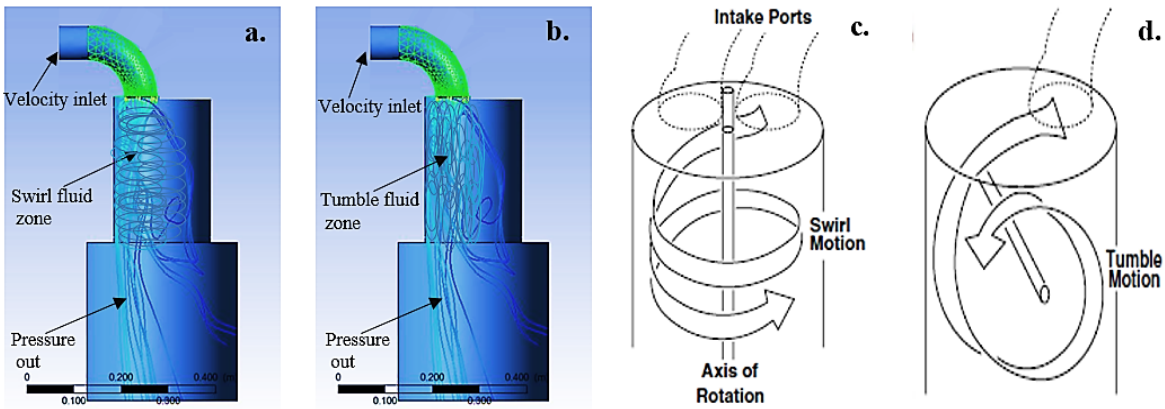

Figure 7. Schematics of boundary condition showing flow movement

$$\frac{\partial}{\partial t}(\rho w)+\frac{1}{r}\frac{\partial}{\partial x}(r\rho uw)+\frac{1}{r}\frac{\partial}{\partial r}(r\rho vw)=\frac{1}{r}\frac{\partial}{\partial x}\left[r\mu\frac{\partial w}{\partial x}\right]+\frac{1}{r^2}\frac{\partial}{\partial r}\left[r^3\mu\frac{\partial}{\partial r}\left(\frac{w}{r}\right)\right]-\rho\frac{vw}{r} \quad (1)$$

$$S_n=\frac{\int rw\vec{v}.d\vec{A}}{\bar{R}\int u\vec{v}.d\vec{A}} \quad (2)$$

$$S_i=\frac{Axial\ flux\ of\ tangential\ momentum}{Axial\ flux\ of\ axial\ momentum*radius}=\frac{2\pi\int_0^R\rho w_t U r^2dr}{R*2\pi\int_0^R\rho WUr^2dr} \quad (3)$$

$$Mass\ conservation=-\frac{\partial}{\partial z}\left(\frac{1}{r\rho}\frac{\partial\psi}{\partial z}\right)-\frac{\partial}{\partial r}\left(\frac{1}{r\rho}\frac{\partial\psi}{\partial r}\right)-w=0 \quad (4)$$

$$Moment\ conservation=-\frac{\partial}{\partial r}\left(r^3\frac{\partial}{\partial r}\left(\frac{\mu w}{r}\right)\right)-\frac{\partial}{\partial z}\left(r^3\frac{\partial}{\partial z}\left(\frac{\mu w}{r}\right)\right)+r^2\left[\frac{\partial}{\partial z}\left(\frac{w}{r}\frac{\partial\psi}{\partial r}\right)-\frac{\partial}{\partial r}\left(\frac{w}{r}\frac{\partial\psi}{\partial z}\right)\right]+r^2g\frac{\partial\rho}{\partial r}+r^2\nabla\left(\frac{v_r^2+v_z^2}{2}\right)=0 \quad (5)$$

$$Energy\ conservation=-\frac{\partial}{\partial r}\left(r\rho D\frac{\partial S}{\partial r}\right)-\frac{\partial}{\partial z}\left(r\rho D\frac{\partial S}{\partial z}\right)+\frac{\partial}{\partial z}\left(S\frac{\partial\psi}{\partial r}\right)-\frac{\partial}{\partial r}\left(S\frac{\partial\psi}{\partial z}\right)=0 \quad (6)$$

where w_t is tangential velocity, μ is mixture viscosity, D is molar diffusivity, U is axial velocity, R is radius of the cylinder, $\bar{R}$ is hydraulic radius, r is radial coordinate, z is radial coordinate, u is axial velocity, w is swirl velocity, v_r is radial velocity, v_z is axial velocity, ψ is variable density stroke function and S is mixture-fraction variable.

3. RESULT AND DISCUSSION

Figure 8 illustrates the variation of piston displacement with time for the same cylinder volume ratio. From the plot, the piston displacement is characterised by sinusoidal wave pattern, indicating a significant or insignificant displacement of the piston for every 0.2 s stroke length made along the cylinder. Practically, the volume which a piston in an ICE cylinder displaces in a single stroke is equal to the distance the piston travels times the internal cross section of the cylinder. In this case, the length of the diameter of a cylinder in an ICE is the bore while the distance travelled by the piston in the cylinder is the stroke. The overall displacement of a reciprocating piston in an engine is determined by multiplying three parameters together: the distance travelled by the piston (the stroke length), the circular area of the cylinder (the bore) and the number of cylinders in the entire engine. The simulation was allowed to run continuously for over 6 minutes in order to observe the piston displacement patterns.

Figure 9 shows the cut out plot from Figure 7 ranging from 0.48-0.64 s. It shows that the force from the power stroke induced an oscillatory motion on the piston from the TDC to the Bottom Dead Centre (BDC). Furthermore, it shows that the power generated from the power stroke was enough to keep the motion throughout the entire cycle without a significant drop in the overall speed of the crankshaft. The simplified diagram shows the time range from 0.48-0.64 s, indicating the smoothness and consistency of the motion per time. The amplitude signifies the piston displacement from TDC to BDC which is also the stroke. One oscillation represents one complete revolution of the crankshaft, therefore, it can be observed that there are four oscillations within about 0.16 s (The range of the plot in Figure 9). The angular speed of the crankshaft can be obtained as 25 rpm. Therefore, the speed is approximately 1500 rpm.

Figure 10 represents a plot of reaction forces against time. The forces appear in the negative section of the plot because the reaction force acts in opposite direction to the expanded forces on the piston. It is important to know that the effect of inertia of the components were also considered in the plot. Thus, the reaction forces are observed to increase and decrease with time due to the power requirement by the engine at various operation intervals.

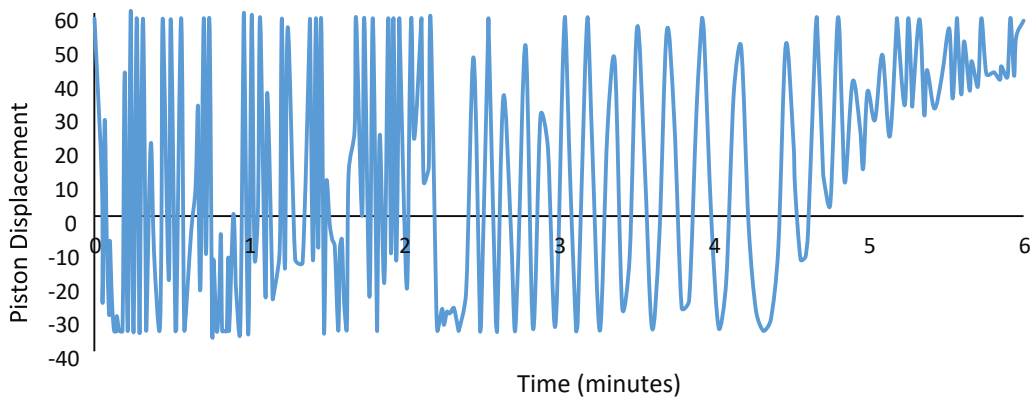

Figure 8. Plot of piston displacement against time

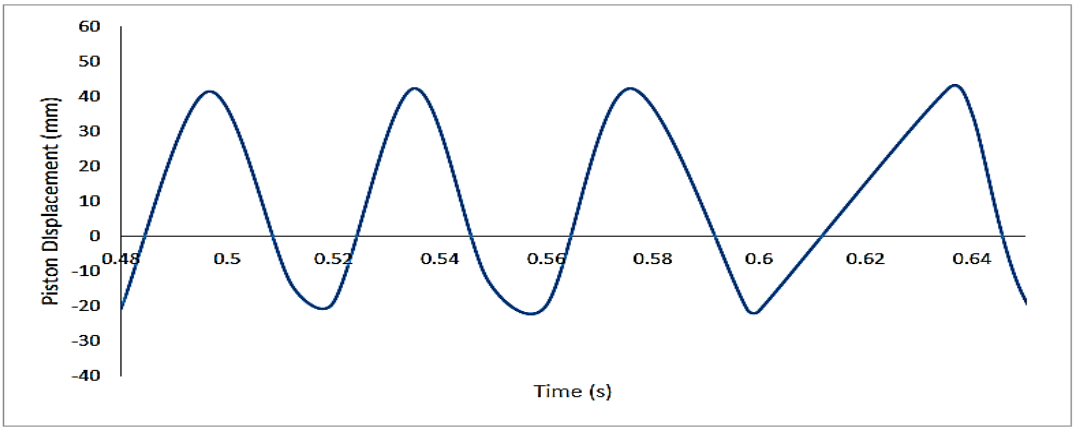

Figure 9. Expanded plot of piston displacement against time

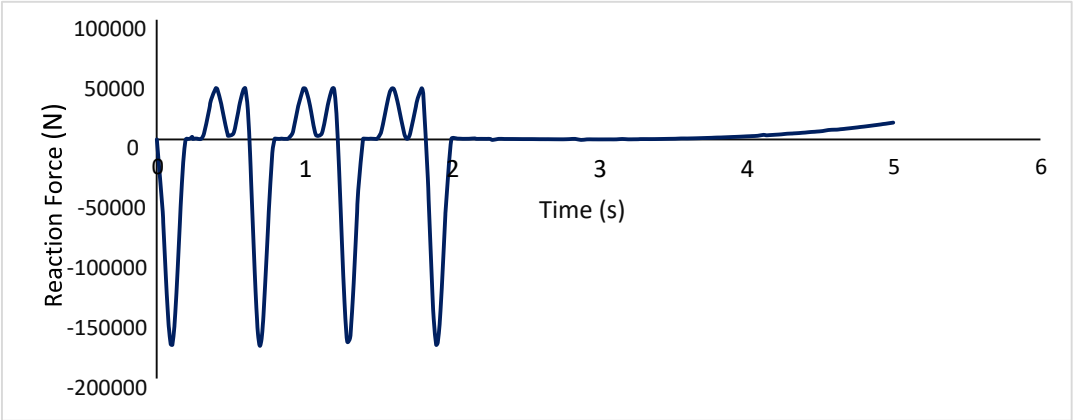

Figure 10. Plot of reaction forces on piston against time

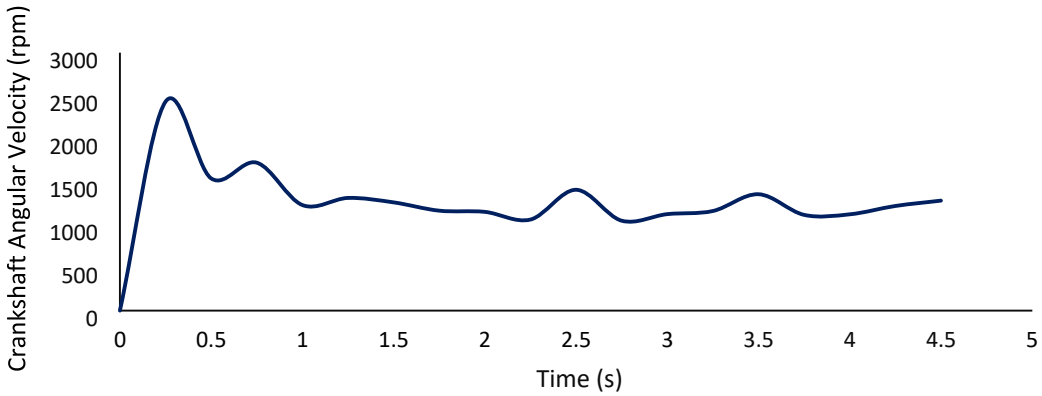

Figure 11. Plot of crankshaft angular velocity against time

Figure 11 shows the angular velocity of the crankshaft when the effect of the forces was extended to 5 s. The angular velocity of the crankshaft shows an initial rise from 0 to 2500 rpm between 0-0.2 s. This is as a result of a sudden rise in speed of the crankshaft due to expansion. The velocity was observed to reduce to 1600 rpm and then increase to 1700 rpm, followed by the same pattern. The fluctuation on speed shows that the flywheel attempted to balance the system. After 1.5 s, the system had a near stable rpm of 1300. Certain power surges from the power or water intake stroke may cause fluctuations as can be observed on the 2.5 s and 3.5 s when the power rises to about 1450 rpm. The speed fluctuations are no greater than 20% in 1.5 s of the stable speed i.e. 1315 rpm. The angular velocity of crankshaft and percentage deviation are presented in Table 2.

Figures 12-14 show the contours of velocity magnitude on ICE Swirl Plane 1, 2 and 3 at 15 mm, 30 mm and 45 mm from TDC set as monitors. The swirl plane contours shows the swirl and tumble characteristics of the fluid. The plot shows that the swirl intensity reduces as the charge moves further down the cylinder. It can also be observed that the charge volume of swirl increases along the cylinder length.

Visuals can be observed in Figure 15 to understand the in-cylinder dynamics as the charge flows down the cylinder on cut plane 1 at 15 mm, 30 mm and 45 mm from TDC. It is observed that an initial velocity of the fluid began to reduce, and thus, the flow rate started declining. It can also be observed that the charge occupies more volume as it flows down the cylinder.

Table 2. Angular velocity of crankshaft and percentage deviation

Start Time (s)	End Time (s)	Angular velocity (m/s)	% deviation
0.00	0.25	2430.972677	87.00
0.25	0.50	1538.615495	18.36
0.50	0.75	1721.602812	32.43
0.75	1.00	1228.492322	5.50
1.00	1.25	1311.13135	0.86
1.25	1.50	1259.551032	3.11
1.50	1.75	1163.014143	10.54
1.75	2.00	1149.178007	11.60
2.00	2.25	1059.418333	18.51
2.25	2.50	1406.16392	8.17
2.50	2.75	1046.332973	19.51
2.75	3.00	1122.661756	13.64
3.00	3.25	1159.202605	10.83
3.25	3.50	1354.434964	4.19
3.50	3.75	1114.020135	14.31
3.75	4.00	1120.547069	13.80
4.00	4.25	1217.596485	6.34
4.25	4.50	1279.935188	1.54

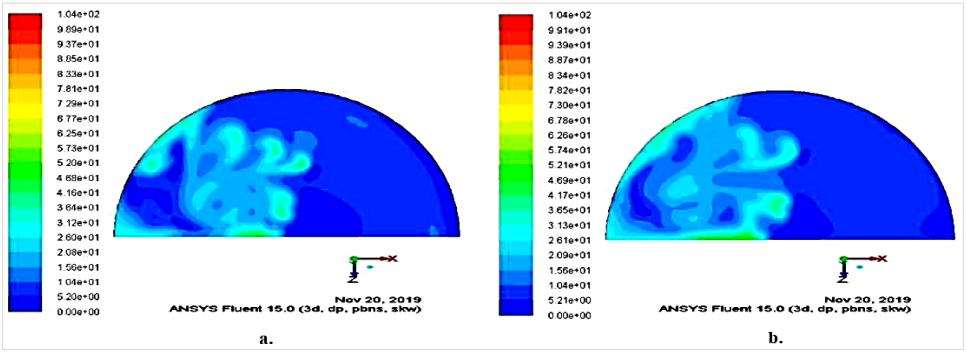

Figure 12. Contours of velocity magnitude on ICE swirl plane 1

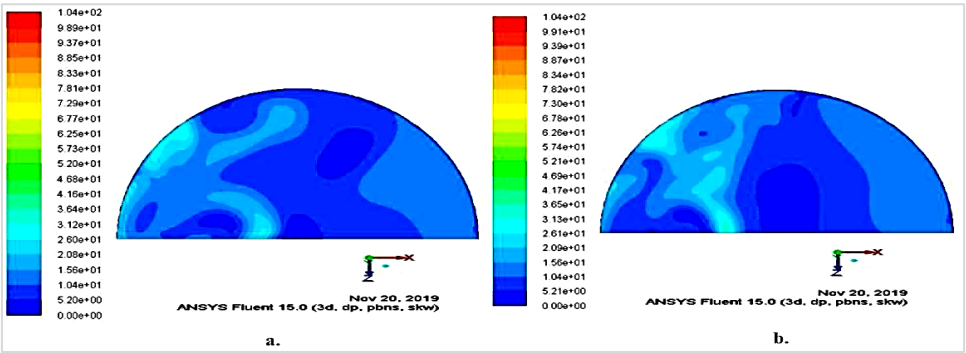

Figure 13. Contours of velocity magnitude on ICE swirl plane 2

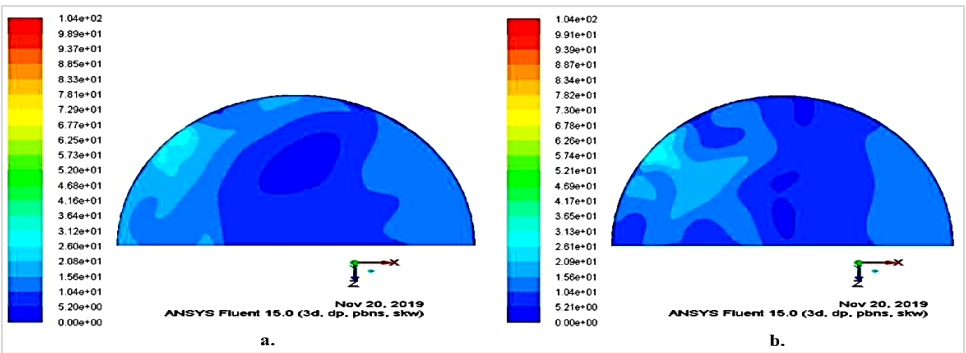

Figure 14. Contours of velocity magnitude on ICE swirl plane 3

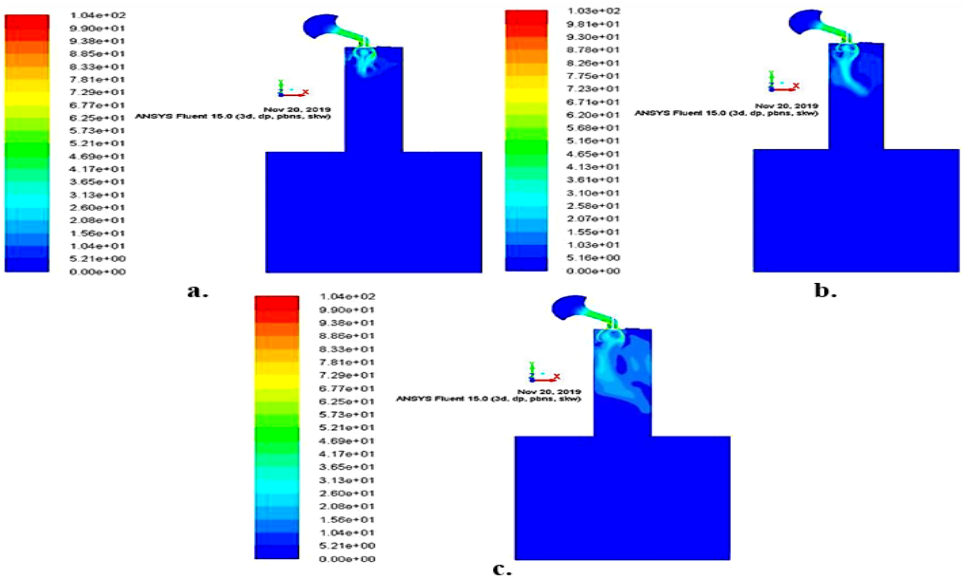

Figure 15. Velocity magnitude on ICE cut plane 1 for (a) 15 mm; (b) 20 mm; (c) 45 mm

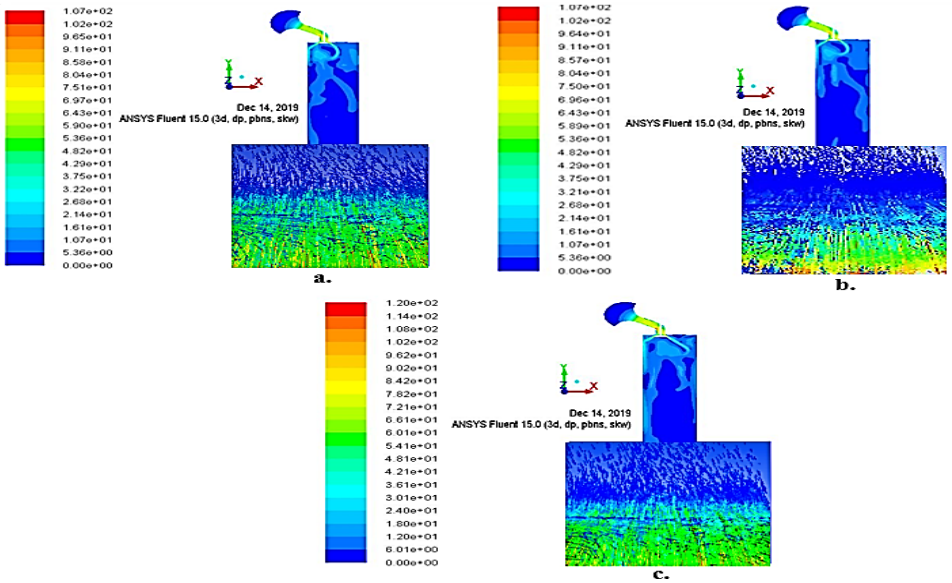

Figure 16. Velocity vector (magnified) on ICE Cut Plane 2 for (a) 15 mm; (b) 30 mm; (c) 45 mm

The velocity seems to be distributed more evenly as the charge travels further away from the TDC and the intensity increases as well. The velocity profile shows the planar profile and cannot show the tumble properties of the fluid, hence, the swirl planes are used to give full understanding of the velocity profile as they show the fluid tumble profile and swirl in the cylinder. The velocities calculated are later utilized by the software to compute the average mass flow rate of the fluid. It was also observed that the velocity increased as the swirl increased. It was also observed that the mass flow rate decreased as the fluid went further away from the poppet valve as shown in Figure 16. Therefore, the intensity of swirl increases along the stroke length of the engine cylinder.

The cut plane monitor searched for planar velocity properties, while the swirl monitors showed the swirl and tumble properties of the fluid. The various monitors were set to give accurate properties of the fluid and monitor the fluid as it flows down the cylinder. The cut and swirl planes were default planes set by ANSYS software. The values are shown for planes of 15, 30 and 45 mm from TDC. The maximum flow rate was calculated at 8 mm as 0.005417 kg/s.

Figure 17 shows the in-cylinder temperature distribution profiles at different swirl numbers. The results indicated that the increasing swirl number of the inlet air from 0.2-0.6 s developed the furnace internal recirculation zone which resulted in the production of combustion materials in the internal recirculation zone. This gives room for effective mixing of fuel and air, which enhances the combustion efficiency by removing the high-temperature zones which is the major reason why nitrogen oxides (NOx) are produced. Moreover, as the swirl number increases, the radial flow distribution improved, and the flame heat exchange area enhanced despite reduction in the maximum flame temperature, which improves the flux radiation efficiency. Due to the increase in swirl number as a result of the decrease in axial velocity component and the increase in its tangential component, the flow expanded radially, resulting in a uniform temperature distribution within the combustion chamber [30].

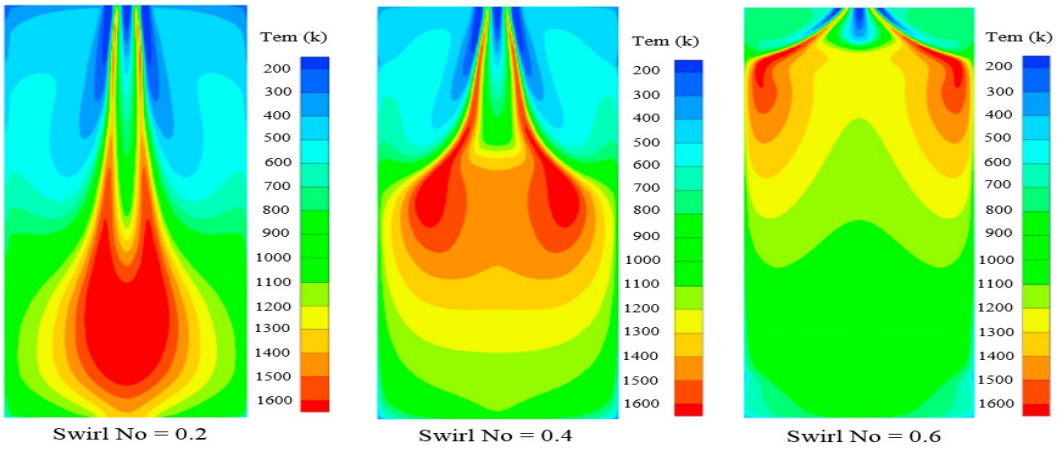

Figure 17. In-cylinder temperature (K) distribution profiles at different swirl numbers

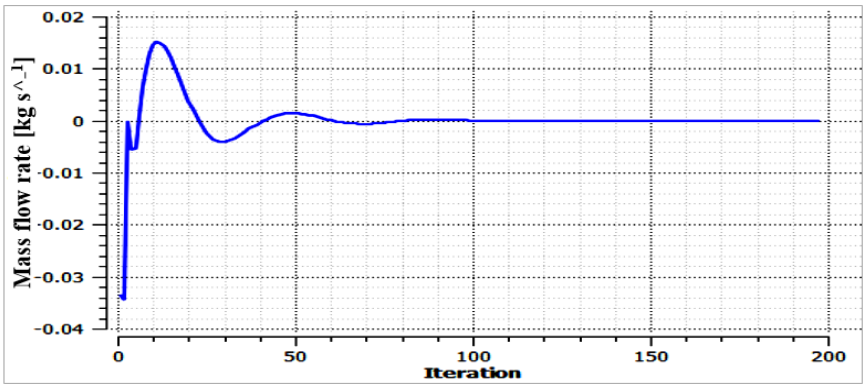

Figure 18. Flow rate (ice_inlet-inplenum1 ice-outlet)

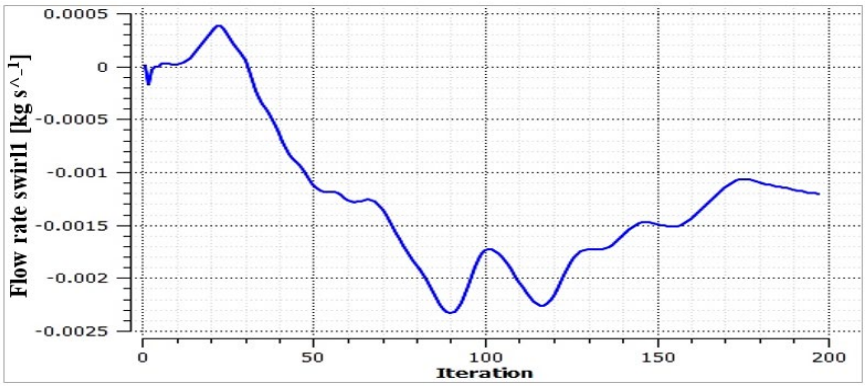

Figure 19. Flow rate monitor on swirl Plane 1 (ice_swirl_plane_1)

Figure 18 shows the mass flow rate plot for the outlet plenum which was observed to have an average value of 0. In the entire simulation, fluctuations were observed from a minimum value of -0.035 to a maximum value of 0.016. The solver indicated that the simulated values were not at a steady state between 0 to about 70 interactions. However from the 70th iterations upward, a steady state value of the mass flow rate was observed on the outlet plenum as 0. This implies that the exhaust valve is closed and no fluid enters through the exhaust port at the time of the simulation.

Figure 19 shows the flow rate on the ice swirl plane 1. The values show negative not because of a reduced velocity, instead it indicates that the charge flows in the negative y direction. An initial flow is observed in the upward direction at early iterations followed by rapid decrease in the flow rate to 0.023 at 90 iterations, rises again to 0.017 at 100 iterations, drops again to 0.017 at 113 iterations and so on. The reason is simply because the monitor measures the area weighted average of the fluid across the swirl plane as the fluid tends to be dispersed further down the cylinder. The fluid also has a corresponding slip on the walls of the cylinder and thus, the overall flow rate reduces.

Figure 20 shows flow rate on the second swirl plane. The plot shows an initial increase in mass flow rate in the upward direction before an increase in the downward direction. The minimum and maximum flow rates fell in the range of -0.0011 and 0.00074 at 90 and 160 iterations. Increased fluctuations are as a result of the distance of the plane from TDC. Hence, mass flow rate measured on this plane is further down the cylinder and the distribution of the charge causes less stability and change the fluid direction. Figure 21 shows the flow rate on swirl plane 3. The plot shows a complete change in direction of the charge.

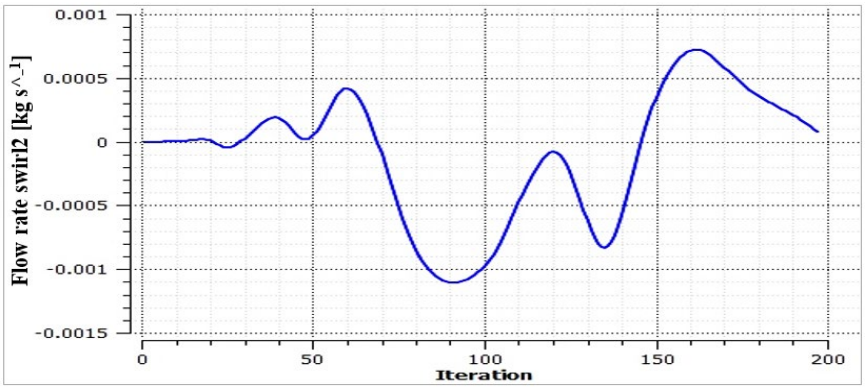

Figure 20. Flow rate swirl on plane 2 monitor (ice_swirl_plane_2)

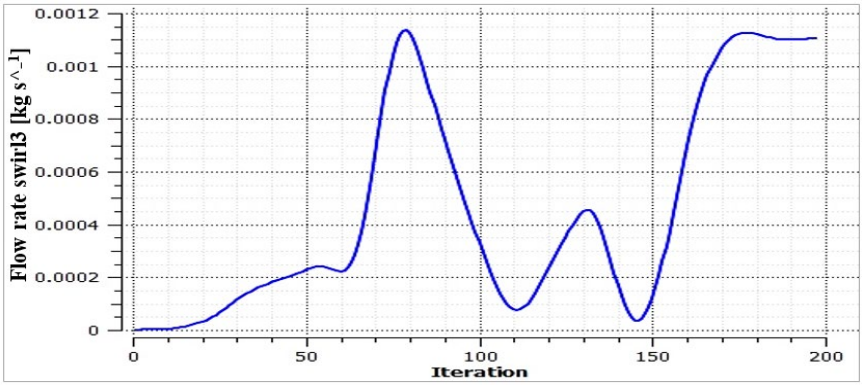

Figure 21. Flow rate swirl on plane 3 monitor (ice_swirl_plane_3_)

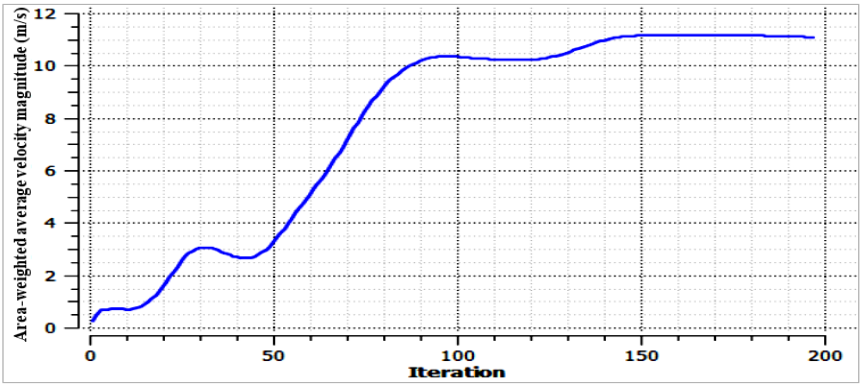

Figure 22. Convergence history of velocity magnitude on ice-int-chamber1-outplenum

It is observed to increase in mass flow rate in the upward direction with no increase in the downward direction. The minimum and maximum flow rates ranged from 0 to approximately 0.0014 at 80 iterations. The overall result is positive due to the distance of the plane from TDC and being further distant from the other planes. Hence, mass flow rate measured on this plane is further down the cylinder. It is observed that the flow is less stable and now lies on the positive axis, though the trend of the plot remains the same. It is expected that more swirl planes will show a lesser range and more accurate results. It can be predicted from the trend that the fluid will show lesser stability over lower ranges.

The plot in Figure 22 shows the convergence history of velocity magnitude on ice chamber 1 out plenum. An increase is observed in the area-weighted average velocity magnitude with increasing number of iterations. As the number of iterations increased, a steady rise coupled with reducing fluctuations was observed. It is observed that the values began to stabilize at 150 iterations. The maximum value of the area-weighted average velocity magnitude is given as 11 m/s with corresponding mass flow rate measured as -0.055479 kg/s.

4. CONCLUSION

In this study, port flow simulation and in-cylinder swirl motion characteristic effects in internal combustion engine duty cycle was successfully carried out using CFD method in ANSYS-FLUENT version R-16. The following conclusions were drawn from the ICE investigation:

a) The air-fuel mixture experienced turbulence as it flowed radially and expanded downwards the ICE cylinder where the flame radiant heat transfer flux eventually increased due to increase in the swirl number, thereby, producing a uniform heat flux distribution in the cylinder.
b) The air-fuel charges entering from the invalve-port undergoes swirling characterised by turbulence and tumbling motion as it expanded towards the cylinder walls, thereby, enhancing combustion process in the cylinder.
c) Increase in the swirl number led to uniform radial temperature distribution as well as reduction in the in-cylinder flame temperature which can reduce the rate of heat loss, expand the heat exchange surface area of the flame within the cylinder walls and also mitigate against the formation of toxic pollutants.

REFERENCES

[1] Z. Barbouchi and J. Bessrour, Turbulence study in the internal combustion engine, *Journal of Engineering and Technology Research*, 1(9), 2009, 194-202.
[2] A. E. Ikpe, I. Owunna, P. O. Ebunilo and E. Ikpe, Material selection for high pressure (HP) compressor blade of an aircraft engine, *International Journal of Advanced Materials Research*, 2(4), 2016, 59-65.
[3] A. E. Ikpe, I. Owunna, P. O. Ebunilo and E. Ikpe, Material selection for high pressure (HP) turbine blade of conventional turbojet engines, *American Journal of Mechanical and Industrial Engineering*, 1(1), 2016, 1-9.
[4] M. P. Kumar and S. Adinarayana, Design optimization of piston of an IC engine and investigation on its influence on overall assembly, *International Journal of Engineering Science and Computing*, 7(6), 2017, 13542-13551.
[5] G. S. Prasas, K. D. Achari, E. K. Goud, M. Nagaraju and K. Srikanth, Design and analysis of internal combustion engine on different materials using CAE tool ANSYS, *International Journal of Engineering and Techniques*, 2(3), 2016, 1-7.
[6] I. B. Owunna and A. E. Ikpe, Design analysis of reciprocating piston for single cylinder internal combustion engine, *International Journal of Automotive Science and Technology*, 4(2), 2020, 30-39.
[7] M. Kaplan, Influence of swirl, tumble and squish flows on combustion characteristics and emissions in internal combustion engine-review, *International Journal of Automotive Engineering and Technologies*, 8(2), 2019, 83-102.
[8] M. Baratta, D. Misul, E. Spessa, L. Viglione, G. Carpegna and F. Perna, Experimental and numerical approaches for the quantification of tumble intensity in high-performance SI engines, *Energy Conversion and Management*, 138, 2017, 435-451.
[9] M. Costa, G. Bianchi, C. Forte and G. Cazzoli, A numerical methodology for the multi-objective optimization of the diesel engine combustion, *Energy Procedia*, 45, 2014, 711-720.
[10] G. Fontana, E. Galloni, E. Jannelli and R. Palmaccio, Influence of the intake system design on a small spark-ignition engine performance: A theoretical analysis, *SAE Technical Paper*, 2003, No. 1-3134-3135.
[11] R. K. Tyagi, S. K. Sharma A. Chandra, S. Maheshwari and P. Goyal, Improved intake manifold design for IC engine emission control, *Journal of Engineering Science and Technology*, 10(9), 2015, 1188-1202.
[12] J. B. Heywood, Fluid motion within the cylinder of internal combustion engines, *ASME Journal of Fluids and Engineering*, 109, 1987, 3-35.
[13] R. F. Huang, C. W. Huang, S. B. Chang, H. S. Yang, T. W. Lin and W. Y. Hsu, Topological flow evolutions in cylinder of a motored engine during intake and compression stroke, *Journal of Fluids and Structures*, 20, 2005, 105-127.
[14] S. Falfari, F. Brusiani and G. M. Bianchi, Numerical analysis of in-cylinder tumble flow structures-parametric 0D model development, *Energy Procedia*, 45, 2014, 987-996.
[15] A. Lakshman, C. P. Karthikeyan and R. Padmanabhan, 3D In-cylinder cold flow simulation studies in an ic engine using CFD, *International Journal of Research in Mechanical Engineering*, 1(1), 2013, 64-69.
[16] D. Mehrnoosh, H. A. Asghar and M. A. Asghar, Thermodynamic model for prediction of performance and emission characteristics of si engine fuelled by gasoline and natural gas with experimental verification, *Journal of Mechanical Science and Technology*, 26(7), 2012, 2213-2225.
[17] A. E. Ikpe and I. B. Owunna, A 3D modelling of the in-cylinder combustion dynamics of two stroke internal combustion engine in its service condition. *Nigerian Journal of Technology*, 39(1), 2020, 161-172.
[18] W. Pulkrabek, *Engineering fundamentals of the internal combustion engine*, New Jersey: Prentice-Hall, 1998.
[19] B. Ramanjulu, A. Fulli, D. J. Raj and A. E. Bekele, Performance analysis of IC engine based on swirl induction by using CFD, *International Journal of Advanced Research in Science, Engineering and Technology*, 2(5), 2015, 622-627.
[20] W. H. Kurniawan, S. Abdullah, K. Sopian, Z. M. Nopiah and A. Shamsudeen, CFD investigation of fluid flow and turbulence field characteristics in a four-stroke automotive direct injection engine, *Journal-The Institution of Engineers, Malaysia*, 69(1), 2008, 1-12.
[21] J. B. Heywood, *Internal Combustion Engine Fundamentals*, New York, USA: McGraw-Hill, 1988.
[22] C. Funk, V. Sick, D. L. Reuss and W. J. Dahm, Turbulence properties of high and low swirl in-cylinder flows, *SAE Technical Paper*, 2002- 01-2841, Warrendale, PA, 2002
[23] S. Lee, K. Tong, B. D. Quay, J. V. Zello and A. Domenic Santavicca, Effects of swirl and tumble on mixture preparation during cold start of a gasoline direct-injection engine, *SAE Technical Paper*, 01-1900, Warrendale, PA, 2001.
[24] M. El-Adawy, M. R. Heikal, A. Rashid, A. Aziz, M. I. Siddiqui, A. Hasanain and A. Wahhab, Experimental study on an IC engine in-cylinder flow using different steady-state flow benches, *Alexandria Engineering Journal*, 56, 2017, 727-736.
[25] C. R. Kumar and G. Nagarajan, Investigation of flow during intake stroke of a single cylinder internal combustion engine, *ARPN Journal of Engineering and Applied Sciences*, 7(2), 2012, 180-186.

[26] H. Kumar and N. Jayashankar, Port flow simulation of an IC engine, *International Journal of Innovations in Engineering Research and Technology*, 2(9), 2015 1-9.
[27] S. Akele, C. Aganama, E. Emeka, Y. Abudu-Mimini, S. Umukoro and R. Okonkwo, CFD port flow simulation of air flow rate in spark ignition engine, *International Journal of Engineering and Management Research*, 10(6), 2020, 87-95.
[28] J. H. Whitelaw and H. M. Xu, Cyclic variations in a lean-burn spark ignition engine without and with swirl, *SAE Technical Paper*, Warrendale, PA, 1995, 950683.
[29] A. E. Ikpe, I. B. Owunna and P. Satope, Finite element analysis of aircraft tire behaviour under overloaded aircraft landing phase, *Aeronautics and Aerospace Open Access Journal*, 2(1), 2018, 34-39.
[30] A. A. Hosseini, M. Ghodrat, M. Moghiman and S. H. Pourhoseini, Numerical study of inlet air swirl intensity effect of a methane-air diffusion flame on its combustion characteristics, *Case Studies in Thermal Engineering*, 18, 2020, 100610.